Vol. 32 No. 135 *Journal of the Radio Research Laboratories* *March 1985*
Printed in Tokyo, Japan *pp. 15–49*

THE BASELINE ANALYSIS OF THE FIRST TEST OBSERVATION BETWEEN JAPAN AND U.S. STATIONS BY USING COMPREHENSIVE K-3 VLBI SYSTEM

By
Fujinobu TAKAHASHI

(Received on December 11, 1984)

ABSTRACT

Radio Research Laboratories (RRL) has developed a high precision Very Long Baseline Interferometer (VLBI), called K-3 system, which is compatible with the Mark-III system of the NASA, U.S.A. K-3 system is also the first comprehensive VLBI system, including the process from the observation through the data analysis. On November 4, 1983, the first VLBI experiment on the trans-Pacific baseline was carried out in close cooperation with NASA. This experiment enabled us to successfully make fringes which showed performance of K-3 system comparable with Mark III system of NASA. The results of this experiment also enabled us to calculate directly the baseline length between Japan and U.S. stations with an accuracy of several decimeters. This direct measurement is an epoch-making event for the Japanese geodetic history. The result also shows the discrepancies of several-meters between observed X, Y, Z coordinates of Kashima and each of the a priori VLBI coordinate-system, (used in East Coast VLBI group in the U.S.A.) and the result of Satellite Laser Ranging (SLR) observed at Shimosato Hydrographic Observatory. These discrepancies suggest the further improvement in the global geodetic system (Japan included) by the accumulation of VLBI data.

Since the accuracy of decimeters in this experiment is due to the smallness of the number of observation, the coming one-day experiment with hundreds of observations will dramatically improve the accuracy. This experiment presented us with a firm base of centimeter-baseline analysis for our coming experiments.

1. Introduction

Since Very Long Baseline Interferometer (VLBI) is essentially independent of the geodetic gravitational effects, it is a unique technique which can calibrate the coordinate system determined by other geodetic methods.

Rogers et al.(1) confirmed the accuracy and the repeatability of the geodetic application of VLBI by using a baseline of 1.2 km. The geodetic applications by VLBI were already summarized in NASA Conference Publication(2), which covered major geodetic applications in 1970's, including the domestic, trans-continental and inter-continental baselines. By the end of 1970's, the new geodesy with an accuracy of centimeter by using VLBI was established by NASA.

Meanwhile, Radio Research Laboratories (RRL) had two experiences of the development of VLBI system called K-1(3) and K-2 systems(4).

K-1 was a tape-recording VLBI system applied to 121 km-baseline and K-2 was a real-time and multi-frequency VLBI system for 46 km-baseline.

Based on the background of experiences mentioned above, RRL and NASA started in 1979 the joint VLBI project for the intercontinental geodetic purposes. The main targets of this project are the detection of plate motions around the Pacific Ocean and North Polar region, the precise determination of earth rotation parameters, and the measurement of regional crustal deformations.

The experiment conducted on Nov. 4, 1983, mentioned here, is the first observation between three stations in the U.S. and Japan to make fringes, which enabled us to confirm the coherence between NASA's Mark III system and K-3 system of RRL. First, this paper describes the conditions of observations, such as participating stations, radio sources, and observation schedules in Chapter 2.

As reported by Saburi et al.(5), the coherence between three stations was successfully detected both by K-3 correlator at Kashima and Mark-III correlator at Haystack. The overview and some details of the preprocessing system both for coherence-detection and bandwidth synthesis are described in Chapters 3 and 4.

The algorithm used for the accurate calculation of a priori models for the least square analysis is summerized in Chapter 5. The theory of data analysis is described in Chapters 6 and 7, separately. Q-R method is applied to the least square analysis of this experiment. The result shows that the data of this experiment are also available for the geodetic application, mainly for the estimation of baseline length with an accuracy of decimeters.

This paper discusses the discrepancies of several-meters between observed X, Y, Z values of Kashima 26 m-antenna and those of the a priori geodetic system. In this paper the results are compared with the preliminary results of satellite laser ranging (SLR) obtained at Simosato Hydrographic Observatory, Japan's Hydrographic Agency.

2. Observation

2.1 Participating stations

Three stations participated in this experiment; those are Kashima (KAS) 26 m, Mojave Base Station (MBS) 12 m, and Owens Valley Radio Observatory (OVRO) 40 m antennas. The a priori X, Y, Z coordinates of those stations in VLBI coordinate system are shown in Table 1 (a). Table 1 (b) shows the baseline components and lengths between three antennas, derived from X, Y, Z in Table 1 (a). Table 1 (b) also shows that both KAS-MBS and KAS-OVRO baselines lie almost along the east-west direction (see Fig. 1 (a).).

Kashima is located in a geophysically active area near the boundaries of three crustal plates (Asian Plate, Pacific Plate, and Philippine Sea Plate) and probably in the part of North American Plate (see Fig. 1 (b)).

Table 1 (a) A priori X, Y and Z coordinates of three participating stations

Stations	X (m)	Y (m)	Z (m)
Kashima (26 m)	−3997895.360	3276579.460	3724116.670
Mojave (12 m)	−2356169.150	−4646756.830	3668471.220
OVRO (40 m)	−2409598.867	−4478350.448	3838603.785

Table 1 (b) A priori x, y and z components of three baselines

Baseline	Bx (m)	By (m)	Bz (m)	Length (m)
KAS – MBS	–1641726.210	7923336.290	55645.450	8091924.228
KAS – OVRO	–1588296.493	7754929.908	–114487.115	7916737.392
MBS – OVRO	53429.717	–168406.382	–170132.565	245276.444

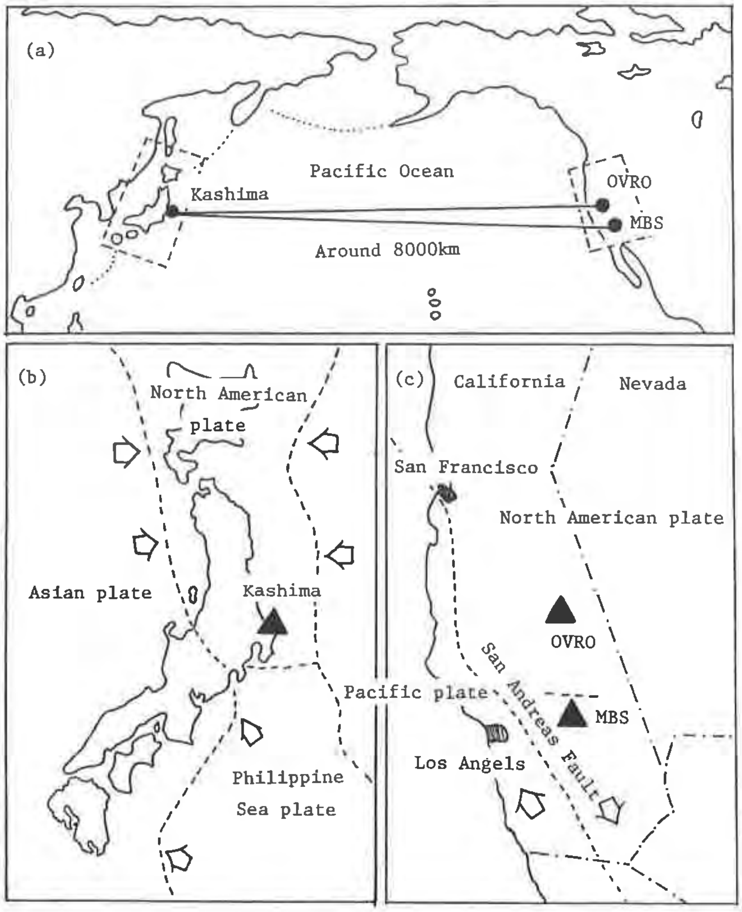

Fig. 1 (a) Participating stations and trans-Pacific baselines

Fig. 1 (b) Three (or probably four) tectonic plates and their boundaries around Kashima

Fig. 1 (c) Major two tectonic plates and San Andreas Fault around California

MBS and OVRO are both located on the east side of San Andreas Fault and they are on North American Plate (see Fig. 1 (c)). San Andreas Fault is considered to be the boundary between North American Plate and Pacific Plate.

2.2 Radio Sources

Since the baseline distance D (around 8000 km) is very long, the fringe beam-width (θ_f: radian) becomes very sharp. It is approximately given by the next equation:

$$\theta_f \simeq \frac{\lambda}{D} \fallingdotseq \frac{3.5\ \text{cm}}{8{,}000\ \text{km}} \Rightarrow 0.9 \text{ milli arc sec}, \quad \cdots\cdots \quad (1)$$

where λ is the wavelength of X band radio wave (8.38 GHz). The correlated flux of a radio source through this interferometer varies complicatedly with an hour angle because of the extra-fine structure of the source. In order to get strong fringes for this sharp beam, we selected three strong radio sources, 4C39.25, 3C273b and 3C345, which are all quasi-stellar objects (QSO).

Table 2 shows the right ascensions and declinations of the radio sources at the epoch of B1950.0 and J2000.0. As mentioned in the following chapters, the epoch of J2000.0 is consistently used in overall K-3 system.

Table 2 Source parameters used for the first US/Japan VLBI experiment

Sources	Right Ascension	Declination	Epoch	Red shift
4C39.25	9h23m55s2943	+39°15′23.8283″	B1950.0	0.699
	9h27m03s01395	+39°02′20.8495″	J2000.0	
3C273b	12h26m33s2460	+2°19′43.4705″	B1950.0	0.158
	12h29m06s6997	+2°03′08.5917″	J2000.0	
3C345	16h41m17s6401	+39°54′10.9911″	B1950.0	0.595
	16h42m58s8099	+39°48′36.9929″	J2000.0	

2.3 Observation Schedules

The experiment conducted on Nov. 4, 1983 and consisted of six observations, spent three tapes for each station, and took two hours and 34 minutes. Three radio sources were observed for twelve minutes each. The schedule of the experiment was kept as simple as possible to maximize chances for us to make fringes and minimize unexpected mistakes.

The first four observations were preprocessed at Kashima and the last two observations were made at Haystack Observatory. Because of the weakness of phase-calibrating tones, Haystack did not try the bandwidth synthesis. Thus the first four observations were used in the following analysis.

Table 3 shows the observation schedule of this experiment. It also shows hour angles, azimuths and elevations, of each source at three stations. At Kashima hour angles of sources are covered the range from −1 h to −7 h, while at MBS/OVRO the range from −3 h to +5 h. The wide range of hour angles and declinations assured, to some extent, independence among the observations.

Table 3 Schedule of experiment: hour angles, azimuths and elevations of the sources

#	UT	Source	Station	Hour angle	Azimuth	Elevation
1	20:00	4C39.25	KAS	−1h04m	71.1°	77.1°
			MBS	+5h41m	302.2°	23.7°
			OVRO	+5h41m	300.9°	25.7°
2	20:40	3C273b	KAS	−3h24m	113.3°	31.8°
			MBS	+3h24m	246.9°	32.2°
			OVRO	+3h19m	244.6°	32.5°
3	21:10	3C345	KAS	−7h10m	48.3°	11.0°
			MBS	−0h20m	39.5°	84.0°
			OVRO	−0h26m	60.3°	84.4°
4	21:40	3C273b	KAS	−2h24m	126.8°	42.2°
			MBS	+4h24m	257.5°	20.6°
			OVRO	+4h19m	255.8°	21.2°
5	22:01	3C273b	KAS	−2h04m	132.5°	45.6°
			MBS	+4h45m	260.8°	16.4°
			OVRO	+4h40m	259.3°	17.2°
6	22:22	3C345	KAS	−5h57m	56.2°	22.5°
			MBS	+0h53m	297.4°	78.7°
			OVRO	+0h46m	289.5°	80.5°

3. Overview of Preprocessing and Analyzing Software

RRL developed the comprehensive K-3 software system on basis of the consistent database system(6). The necessity of the consistent database has been repeatedly pointed out by Ma(7) and Yoshino et al.(8), because the VLBI data analysis needs the long-term managements of VLBI data in large amount and of various kinds. In order to satisfy these requirements, RRL developed a network-type database management system KASTL(8) and backup-utilities(9) to maintain or update KASTL.

Mark-III software system was thoroughly investigated to design the new K-3 software system. Fig. 2 shows the rough sketch of the K-3 software system. This system mainly consists of three groups: preprocessing group, analyzing group, and database system KASTL.

The preprocessing group consists of three parts of software: cross-correlation software KROSS(10), bandwidth synthesizing software KOMB(11) and data-transformation software KONV(12).

By synchronizing two or more data recorders, KROSS controls K-3 cross-correlating processor. KROSS acquires a large amount of cross-correlation data and stores onto the disc of host computer HP/1000 as mentioned in Sec. 4-1. KOMB synthesizes these correlation data through both coarse-search and fine-search processes, and it determines the observed delay and delay rate precisely. The algorithm used in KOMB is described in Chapter 4.

The analyzing group mainly consists of three parts of software, namely database-setup software KASET(13), a priori model software KAPRI(14) and baseline analyzing software KLEAR(15).

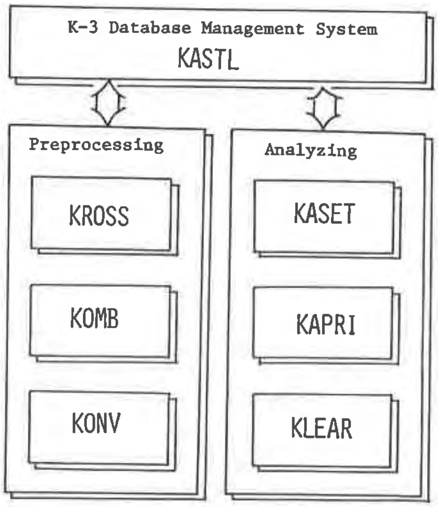

Fig. 2 Overview of K-3 preprocessing and analyzing software system

KASET places the database items, for example, information of weather, planetary ephemerides or earth rotation parameters onto KASTL. Those items are necessary both in preprocessing and analyzing groups. KAPRI calculates a priori delays, delay rates, and their partial derivatives with regard to the adjustment of parameters. International Latitude Observatory of Mizusawa (ILOM) and Geographical Survey Institute (GSI) supported us in making some of the a priori physical models.

KLEAR estimates the baseline vectors, the clock offsets among the stations, and the earth rotation parameters by the least square method. It adjusts "C"alculated value (C: calculated by KAPRI) to explain the "O"bserved values (O: determined by KOMB).

Besides these two groups, K-3 database is maintained by many utilities.

4. Preprocessing

A most likelihood method to decide the delay time between two Gaussian noises is to minimize the next square integral Q (τ), which shows the square errors between two noises(16).

$$\operatorname*{Min}_{\tau}\,[Q(\tau)] = \operatorname*{Min}_{\tau}\,[\int_{-\infty}^{\infty} \left\{X(t) - Y(t+\tau)\right\}^2 dt]\ , \quad \ldots\ldots\ldots\ldots \quad (2)$$

where, X (t) and Y (t) are two Gaussian noises, including some coherent components. Eq. (2) can be expanded to three terms as follows:

$$Q(\tau) = \int_{-\infty}^{\infty} X^2(t)\,dt + \int_{-\infty}^{\infty} Y^2(t+\tau)\,dt - 2\int_{-\infty}^{\infty} X(t)\,Y(t+\tau)\,dt. \qquad (3)$$

The first term is independent of τ; this is a constant. The second term is also independent of τ, because the integration limits are always far larger than τ. Thus, Eq. (2) is equivalent to maximizing the cross-correlation function $R_{xy}(\tau)$, as follows:

$$R_{xy}(\tau) = \int_{-\infty}^{\infty} X(t)\,Y(t+\tau)\,dt. \qquad (4)$$

The cross-correlation and bandwidth synthesis are the methods to search such a delay to maximize $R_{xy}(\tau)$; the delay is equivalent to the most likelihood value of delay.

4.1 Data Compression through Preprocessing

On this experiment, the received signals of eight channels were sampled at the rate of 4 mega bits/sec for each observation; they are integrated and synthesized for 120 seconds in preprocessing. The total amount of integration data reaches up to 3.84 giga bits.

Through preprocessing, we can improve the signal to noise ratio of a coherent flux to the system noise, and skim the desired precise information of delay. Fig. 3 shows the sequential data compression by preprocessing.

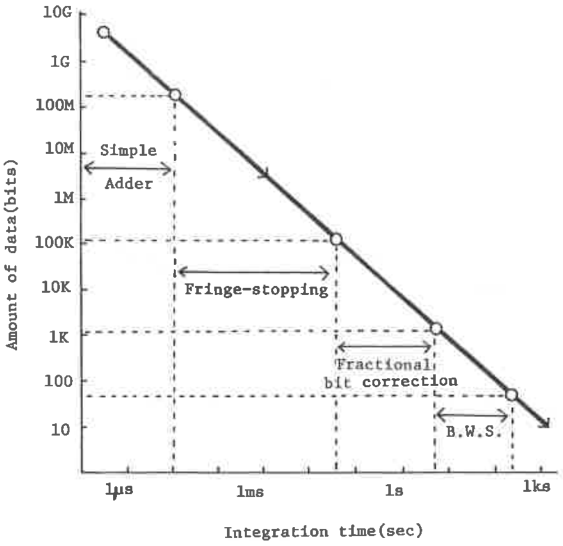

Fig. 3 Data compression through sequential preprocessing (B.W.S.: bandwidth synthesis)

The first step is a simple accumulation by binary counters. To compensate Doppler shift by earth rotation, the integration with fringe-rotation (or fringe stopping) is utilized in the second step; a three-level-fringe-pattern shown in Fig. 4 balances the fringe phase. The third step is a fractional-bits integration to recover the small loss of the coherence power just at the occurrence time of bit-shifts. And the last step is a bandwidth synthesis (B.W.S.) using 2-dimensional Fourier transformations.

The boundaries among these four steps are determined by the fringe-period, the bit-shift-period, and the maximum integration time in K-3 correlation processor. In the case of 3C273b of this experiment, the periods of fringe and bit-shift are about 62 micro-seconds and 126 milli-seconds, respectively, and the maximum integration time is 4 seconds.

Fig. 4 is a schematic figure of the data compression through preprocessing. The raw-data bits, sampled at 4 megabits/sec, are simply accumulated for 30–80 bits at the first stage. Three-level fringe pattern consists of the positive, zero, and negative levels. On the positive level, all the binary counters of K-3 correlator accumulate the data positively. At the negative stage, the accumulating results by the counters are subtracted from the total integrator. On the zero level, the accumulation counters stop and no effect appears in the total integrators. In K-3 correlator, the fringe rotation is controlled in a programmable way by a host computer.

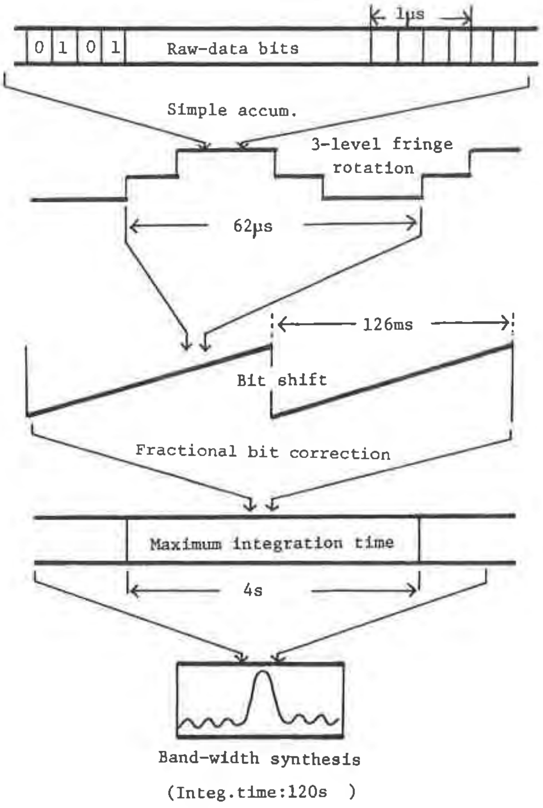

Fig. 4 Schematic figure of data compression in preprocessing

Rotating the three-level pattern, we can integrate the accumulated data up to 126 msec (period of bit-shift). At the timing of the bit-shift of the programmable delay, n x 90°-phase jumps are available to decrease the coherence-loss. This technique is called "fractional-bit compensation".

Compensating the fractional bits, K-3 correlator can integrate the total amount of data up to 4 seconds. The integrations, above mentioned, compress the raw data into one hundred millionth (10^{-8}). Since the further improvement in S/N is difficult in the hardware, the software for bandwidth synthesis, mentioned in Sec. 4.4, is used for the further integration.

4.2 Cross Correlation

The tape-recording VLBI system always needs the synchronization between two or more data recorders before and throughout the cross correlation. K-3 correlator reads the time-codes of the reproducing signals from data recorder and it changes the transporting velocity of one data recorder, referring to the time-codes of the other. At the synchronized stage, the difference between the two time-codes is within 1,000 bits (250 micro-seconds). The data recorders (Honeywell Model 96) and software KROSS have special designs to make the quick synchronization, despite of very high speed of tape (3.43 meters/sec). Since the data consumed for the synchronization cannot be used for the cross-correlation, they should be considered to be the loss of data. In this case we reduced the loss to around 2%(17).

It is necessary to provide K-3 processor with two kinds of parameters, namely delay-parameters and phase-parameters. The delay-parameters mainly consist of three parameters which are a delay-bit-lag, an initial phase of fractional bit, and a period of bit-shift. In the phase-parameters there are also three major parameters: those are an initial phase, a fringe rate, and a fringe acceleration. Since the phase parameters depend on the receiving frequency, each correlating channel needs the respective phase-parameters. These correlation parameters of KROSS are calculated through the same algorithm as used in KAPRI of the analyzing software. The consistency of algorithm between KROSS and KAPRI, as mentioned in Chapter 5, is very distinguished feature of K-3 system, and it saved time to develop and debug both KROSS and KAPRI. This consistency, based on the comprehensive database KASTL, also helped the feedback of the calculating results to and from each other.

The preprocessed data from K-3 correlator are stored in the cross-correlation data files on the disc of HP1000/45F computer system. Since one observation produces one data file, the typical one-day schedule produces more than one hundred files per baseline. To prevent the confusion of files, the database KASTL manages their names.

4.3 Coarse Processing

In the cross-correlation data file, there is a three-dimensional complex array indexed by m (m=1-8:bit lag), k (k=1-n:integration time), and n (n=1-N:synthesizing frequency of each channel). One component of this array is given by the following expression:

$$R(m,k,n) = R_{\cos}(m,k,n) + iR_{\sin}(m,k,n), \quad \cdots\cdots \quad (5)$$

where $R_{\cos}$ and $R_{\sin}$ are the real and imaginary parts of R, corresponding to the cosine and sine components of fringe stopping pattern, respectively.

The first step of the synthesis is called "coarse processing". In order to integrate coarsely, we have to make Fourier transform of Eq. (5) with regard to the bit-lag m, thus the video-cross spectrum S (j, k, n) is given by the following equation:

$$S\,(j,k,n) = \frac{1}{8}\sum_{m=1}^{8} R\,(m,k,n)\exp\,(-i\omega_j^{v}\, m\, \tau_s), \qquad \ldots\ldots\ldots\ldots\ldots\ldots \quad (6)$$

where ω^{v}_j is j-th angular-frequency dividing the video bandwidth (0–2 MHz) into eight parts, and τ_s = 250 ns. The coarse search function F (n, $\Delta\tau$, $\Delta\dot{\tau}$) of n-th channel is calculated as follows:

$$F\,(n,\Delta\tau,\Delta\dot{\tau}) = \sum_{j=1}^{8}\sum_{k=1}^{k} S\,(j,k,n)\exp\,(-i\omega_0^{\,n}\Delta\dot{\tau}\,\Delta t\cdot k)\exp\,(-i\omega_j^{v}\Delta\tau), \qquad \ldots\ldots \quad (7)$$

where $\Delta\tau$ and $\Delta\dot{\tau}$ are the search parameters in delay domain and delay rate domain, respectively. $\omega_0^{\,n}$ is the receiving angular-frequency of n-th channel and Δt is a time unit (nominally 2 or 4 seconds) for the correlation data-output. F (n, $\Delta\tau$, $\Delta\dot{\tau}$) is equivalent to the cross correlation function R_{xy} considered in Eq. (4).

Since there exists a two-dimensional Fourier transform in Eq. (7), it is very easy to calculate this equation by two-dimensional FFT. The total summation of absolute value of F (n, $\Delta\tau$, $\Delta\dot{\tau}$) with regard to channel n is called "Coarse search function". The maximization of this function, as shown in the next equation, corresponds to the coarse synthesis, in which the phase calibration of an each channel being neglected.

$$\underset{\Delta\tau,\Delta\dot{\tau}}{\mathrm{Max}}\ [\sum_{n=1}^{N} |\,F\,(n,\Delta\tau,\Delta\dot{\tau})|\,] \Rightarrow \Delta\hat{\tau},\ \Delta\hat{\dot{\tau}}, \qquad \ldots\ldots\ldots\ldots\ldots\ldots\ldots\ldots \quad (8)$$

where $\Delta\hat{\tau}$ and $\Delta\hat{\dot{\tau}}$, searched through Eq. (8), will be adopted as the new a priori values of delay and delay rate in the bandwidth synthesis. Fig. 5 shows that the coarse-search aligns phase-vectors straightforwardly both in delay and delay rate domain.

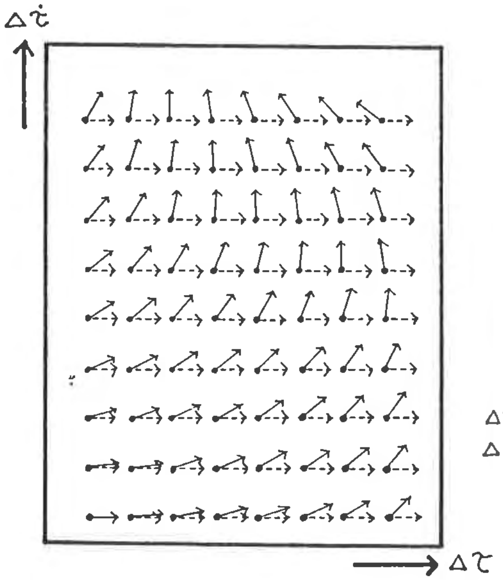

$\Delta\tau$:Delay search parameter
$\Delta\dot{\tau}$:Delay rate search parameter

Fig. 5 Distribution of phases before (solid-line) and after (dotted line) the coarse processing

The important role of coarse processing is to detect the cross-correlation power of radio sources' signal against the ambient noises. It is often difficult to get the big signal-to-noise ratio enough to detect fringes in the single 2 MHz channel. Thus it is necessary to upgrade the S/N of fringes by integrating both in time and frequency-domain. The coarse processing is often suitable and sensitive for this purpose. We used this search to detect the fringes with large S/N for all six observations at three baselines. This allowed us to confirm the fundamental success of the experiment.

Fig. 6 (a) shows an example of coarse-search function for the quasar 3C345. Since S/N of 3C345 was enough high, the peak-search of the function was succeeded with an accuracy of 20 ns.

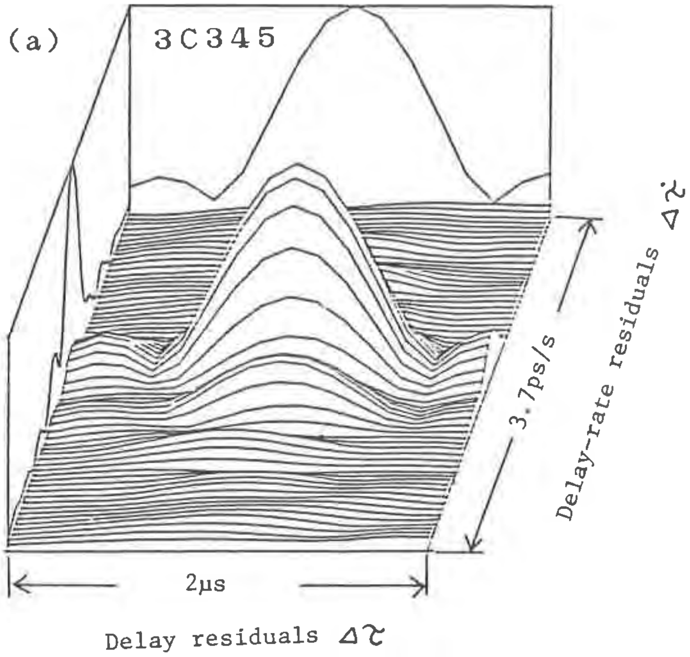

Fig. 6 (a) An example of a coarse-search function (3C345, 21:10 UT, Nov. 4, 1983)

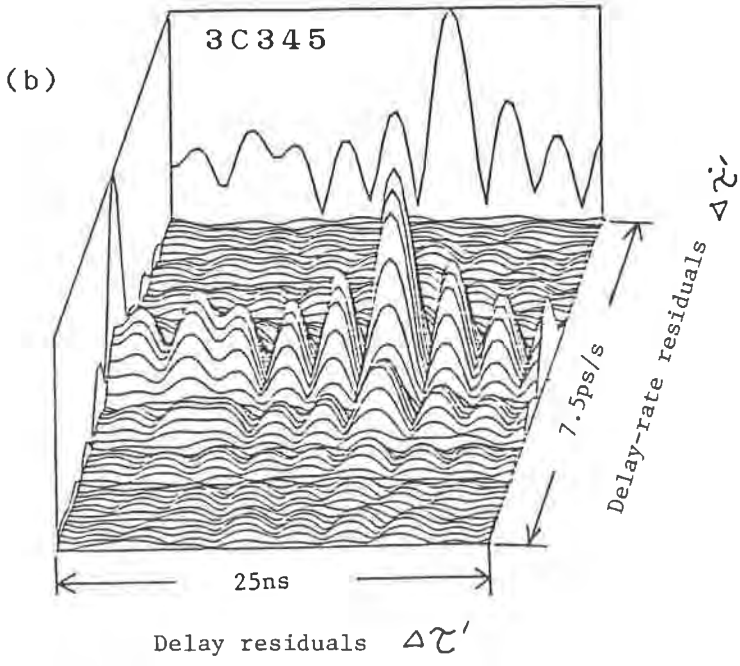

Fig. 6 (b) An example of a fine-search function (3C345, 21:10 UT, Nov. 4, 1983)

4.4 Bandwidth Synthesis

The delay residual $\Delta\hat{\tau}$ and the delay rate residual $\Delta\hat{\dot{\tau}}$, obtained through the coarse processing, are used as a priori values for the bandwidth synthesis:

$$D(\Delta\tau', \Delta\dot{\tau}') = \sum_{n=1}^{N} \sum_{k=1}^{K} \sum_{j=1}^{8} S(j, k, n) \cdot$$
$$\exp\left[i\left\{\omega_j{}^{v}\Delta\hat{\tau} + \omega_0{}^{n}\left[(\Delta\hat{\dot{\tau}} + \Delta\dot{\tau}')\Delta t\cdot k + \Delta\tau' + \Delta\phi_n\right]\right\}\right], \quad \cdots\cdots\cdots\cdots\cdots\cdots \quad (9)$$

where $D(\Delta\tau', \Delta\dot{\tau})$ is called as the fine-search function with regard to new parameters, $\Delta\tau'$ and $\Delta\dot{\tau}'$. The bandwidth synthesis gives us the fine residuals $\Delta\hat{\tau}'$ and $\Delta\hat{\dot{\tau}}'$ to maximize the amplitude of Eq. (9), where $\omega_0{}^{n}$ and $\Delta\phi_n$ are a receiving frequency and a calibrated phase of the n-th channel, respectively. Fig. 6 (b) shows an example of the fine-search function for the quasar 3C345. This function enables us to calculate the fine-search residuals within an error of 0.1 ns. Fig. 7 illustrates how the fine-search aligns multi-frequency phase-vectors and how the length of vector summation of all frequencies is maximized.

Using both coarse and fine residuals $\Delta\hat{\tau}$, $\Delta\hat{\dot{\tau}}$ and $\Delta\hat{\tau}'$, $\Delta\hat{\dot{\tau}}'$, the maximum likelihood delay $\hat{\tau}_0$ and delay rate $\hat{\dot{\tau}}_0$ are calculated by the following equations:

$$\hat{\tau}_0 = \tilde{\tau}_0 + \Delta\hat{\tau} + \Delta\hat{\tau}' \qquad (10)$$

$$\hat{\dot{\tau}}_0 = \tilde{\dot{\tau}}_0 + \Delta\hat{\dot{\tau}} + \Delta\hat{\dot{\tau}}', \qquad (11)$$

where $\tilde{\tau}_0$ and $\tilde{\dot{\tau}}_0$ are the calculated values of delay and delay rate, respectively. The maximum likelihood delay $\hat{\tau}_0$ is referred to as "O:observed value" in the following Chapters.

Table 4 shows the first four observed delays processed at Kashima and their S/N errors of the delay in X-band for this experiment. (Since phase-calibration signal was weak in X-band, Haystack did not search the fine-residuals of last two observations.) If the closure errors, which are the results added in a cyclic manner as "KAS-MBS"-"KAS-OVRO"+"MBS-OVRO", are around sub-nanoseconds, the bandwidth syntheses are considered to be successful. The closure errors often have some ambiguities of n x 100 ns or n x 10 ns. The ambiguities usually come from the periodicity of fine-search function with regard to delay$^{(11)}$. After the corrections of the ambiguities, the residuals are smaller than 0.3 ns, as shown in Table 4; the observed delays are precise enough to judge the experiment to be successful.

Table 4 Observed delays, S/N errors and closure errors (ns)

#	Source	KAS-MBS "K – M"	KAS-OVRO "K – O"	MBS-OVRO "M – O"	Closure error Raw	Closure error Correct
1	4C39.25	11,874,815.328	11,237,436.866	–637,368.745	9.717	–0.283
		+/–.120	+/–.069	+/–.018		
2	3C273b	–633,806.005	–686,765.918	–52,960.046	0.133	0.133
		+/–.037	+/–.021	+/–.002		
3	3C345	–17,343,635,191	–17,338,173.355	5,361.533	–100.303	–0.303
		+/–.048	+/–.024	+/–.006		
4	3C273b	6,385,280.151	6,181,594.724	–203,685.141	0.286	0.286
		+/–.038	+/–.022	+/–.003		
5	3C273b	–	–	–	weak p-cal.	
6	3C345	–	–	–	weak p-cal.	

5. Physical Models

It is commonly believed that VLBI is the most accurate geodetic technique in measuring a long distance. The analysis of VLBI data requires many kinds of astronomical, geodetic, and geophysical models to calculate the a priori values with the highest precision$^{(7)}$.

Our a priori model software KAPRI is based on the following three premises:

(1) Time system: TBD (Barycentric Dynamical Time, Aoki et al., 1982) is adopted as a time-reference system. TBD is equivalent to the relativistic coordinate time (CT) at the

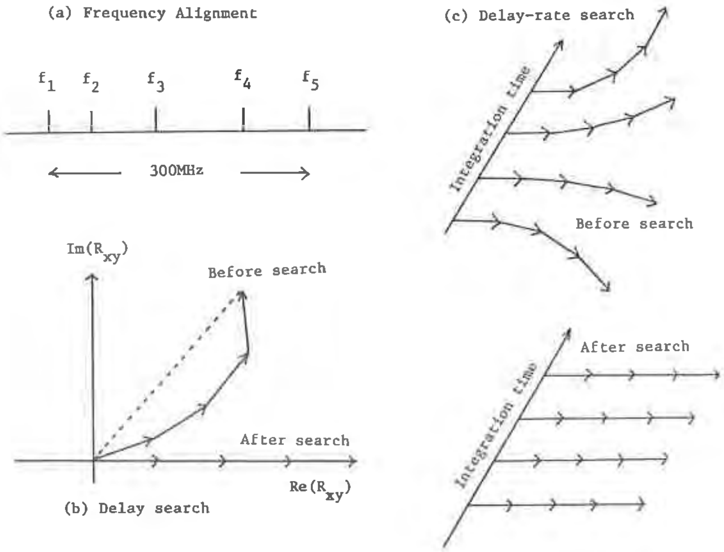

Fig. 7 Schematic illustration of phase-vectors' alignments before and after the fine processing

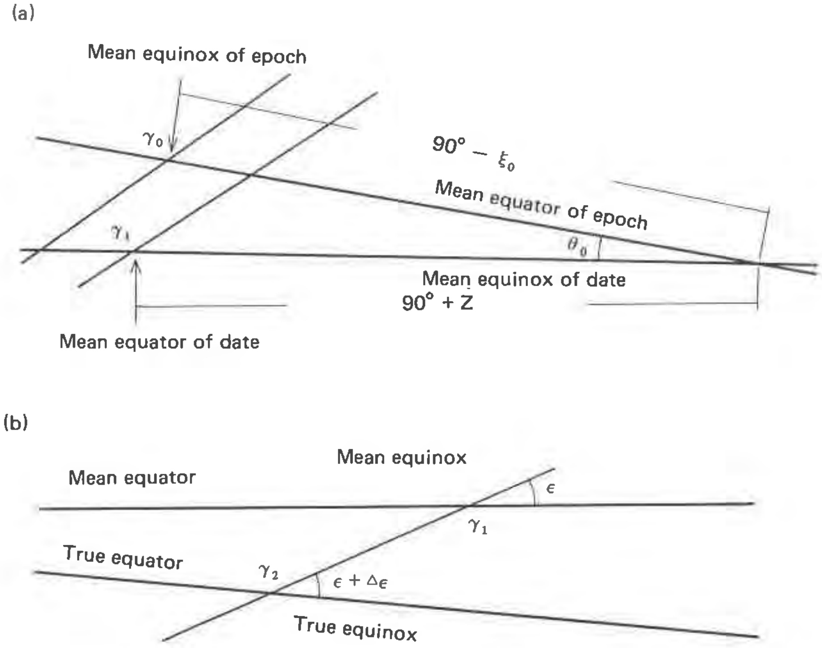

Fig. 8 The diffinitions of precession (Fig. 8 (a)) and nutation (Fig. 8 (b)) parameters

barycenter of Solar System. TBD is also equivalent to the Ephemeris Time (ET) by adding appropriate constant time.

(2) Epoch: J2000.0 system is adopted in the overall K-3 system instead of the conventional B1950.0 system.

(3) Spin axis of earth: Mean axis of figure is adopted for the reference spin axis of the earth, instead of the instantaneous spin axis. Thus the diurnal polar motion, called "Opoltzer Term", is neglected in our model.

Based on these premises, RRL designed the new physical model software KAPRI in cooperation with International Latitude Observatory of Mizusawa (ILOM) and Geographical Survey Institute (GSI).

KAPRI consists of three groups of physical models. Those relate to the inertial reference frame, the earth-fixed coordinate system, and the propagation effects.

5.1 Inertial Reference Frame

To describe the a priori geometrical delay precisely, we have to transform the earth-fixed coordinate system of date into the inertial reference frame. The transformation of mean axis of figure consists of the precession matrix P, the nutation matrix N, the diurnal rotation matrix S, and the polar motion matrix W:

(1) Precession

KAPRI adopts Lieske's$^{(18)}$ precession model whose argument of time is Julian centuries T from epoch J2000.0 (JD2451545.0). This model transforms the coordinate system from J2000.0 into the mean position of date. Using precession parameters by Lieske: z, ξ_0, θ_0 illustrated in Fig. 8 (a), we can calculate the precession matrix P by the next equation:

$$P = R_Z(z)\, R_Y(-\theta_0)\, R_Z(\xi_0), \quad \cdots\cdots (12)$$

where R_Y and R_Z are rotation matrices around the Y and Z axes, respectively.

(2) Nutation

It is necessary to calculate the nutation matrix to transform the mean position of date to the true position of date. KAPRI adopted Wahr's$^{(19)}$ nutation table with 106 terms. His table contains all the terms of the nutation of longitude, larger than 0.0001″, and its size is 80% larger than Woolard's one which has been used commonly. The time argument T of this model is the same as Lieske's one.

By using Wahr's table, KAPRI calculates the nutation of longitude $\Delta\psi$ and the nutation of obliquity $\Delta\epsilon$, as illustrated in Fig. 8 (b). The nutation matrix N is given by the following equation:

$$N = R_X(\epsilon + \Delta\epsilon)\, R_Z(\Delta\psi)\, R_X(-\epsilon). \quad \cdots\cdots (13)$$

(3) Earth Rotation

The earth rotation matrix S is equivalent to the counter-clockwise rotation for the angle of the Greenwich apparent sidereal time GAST around Z-axis. Then,

$$S = R_Z(-\mathrm{GAST}), \quad \cdots\cdots (14)$$

where $$\mathrm{GAST} = \mathrm{GMST} + \nu \cdot \mathrm{UT1} + \Delta\psi \cos \epsilon, \tag{15}$$

$$\mathrm{GMST} = 6\mathrm{h}41\mathrm{m}50\mathrm{s}.\,5484 + 8{,}640,\ 184\mathrm{s}.\,8129 \times T + 0\mathrm{s}.\,0931 \times T \times T, \tag{16}$$

ν is the scaling coefficient from the universal time to the sidereal time and ϵ is the mean obliquity of date of the ecliptic.

The a priori UT1 used in Eq. (15) is reported by IPMS and BIH periodically. The earth rotation parameters are here regarded as unadjusted ones because of the shortness of the number of observations, although UT1 and polar motions are to be determined by VLBI techniques with more observations.

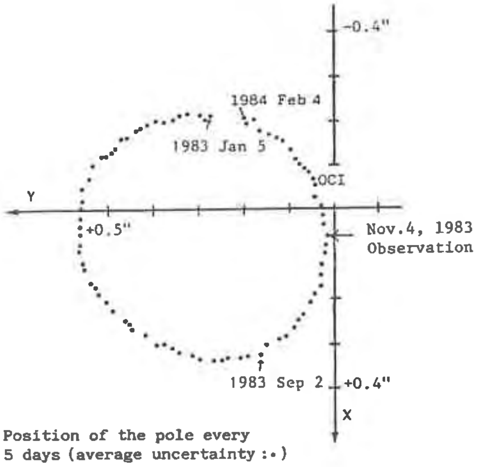

Fig. 9 The plots of a priori polar motion reported by MERIT news letter

(4) Polar Motion

The polar motion matrix W is given by the following equation:

$$W = R_x(-y)\, R_y(x), \tag{17}$$

where x, y are two components of polar motion reported by IPMS or BIH.

The baseline vector $\underline{B}_{fix}$ in the earth-fixed coordinate is transformed into the inertial reference frame $\underline{B}$ by the next equation.

$$\underline{B} = P^T N^T S^T W^T \underline{B}_{fix}. \tag{18}$$

The accuracy of earth rotation parameters (ERPs) will be discussed later so if they can be regarded as unadjusted parameters. Table 5 shows the contribution of ERPs to the error of calculated delay. Chapter 9 will provide the error analysis including these ERPs' effects.

Table 5 Partial derivatives with regard to earth rotation parameters

Partials	Obs. #	KAS-MBS	KAS-OVRO	MBS-OVRO
$\partial\tau_g/\partial w_x$ (ps/m.a.s)	1	−16.1	−17.6	−1.4
	2	−00.1	−02.8	−2.6
	3	−16.8	−17.0	−1.9
	4	−00.1	−02.8	−2.7
$\partial\tau_g/\partial w_y$ (ps/m.a.s)	1	80.5	79.7	−0.9
	2	5.0	4.3	−0.7
	3	82.8	79.0	−3.7
	4	4.8	4.8	−0.0
$\partial\tau_g/\partial UT1$ (ns/ms)	1	1.26	1.24	0.03
	2	1.97	1.92	0.04
	3	0.82	0.79	0.02
	4	1.91	1.87	0.04

5.2 Earth-fixed Coordinate System

Since the conventional geodetic methods determine the station position by referring to the direction of the gravitational vector, it is difficult to position an antenna globally by using this method. VLBI is quite a unique technique which makes the calculation of baseline vectors possible directly without the information of the gravitational field. VLBI is considered to be very important technique for colocated observation with the conventional techniques in order to calibrate them.

As the a priori coordinates of Kashima, we adopted the Tokyo Datum (Besselian geodetic system). The transformation described in Appendix A was used to calculate the a priori global position of Kashima through the WGS-72 system.

Since earth tide and ocean loading perturb the station-position, we need the precise models to compensate them. KAPRI adopted the models developed by ILOM and supported by GSI. The outline of these models is as follows:

(1) Earth tide: KAPRI adopted Wahr's earth tide model compatible with his nutation model.

(2) Ocean loading: KAPRI adopted Schwiderski's global ocean tide model and GSI's coastal line data around Japan.

The details of these model should be referred to Takahashi, Y. et al.(14)

5.3 Propagation Effects

As the propagation effects, we generally consider the non-dispersive effects by the neutral (dry and wet) atmosphere, the dispersive effects by the solar corona and the ionosphere, and the pass-bending through the solar gravity field. Considering the decimeter-accuracy of this experiment, one pays attention to the two big effects as follows:

(1) Dry atmosphere: The zenith excess path L_d is calculated by Moran's(20) model:

$$L_d = 77.6E{-}6 \times R \times P_0/g/m \quad \ldots\ldots (19)$$

where R (= 8.3144 N/deg/mol) is universal gas constant, P_0 (milli bar) is a partial pressure of dry atmosphere, g (= 9.80 m/sec^2, dependent on position) is a gravitational acceleration and m is a mean molecular weight of the dry atmosphere (= 0.028966 kg/mol). The excess path length L through the line of sight with the elevation Eℓ is calculated by Chao's$^{(21)}$ model as follows:

$$L = \frac{L_d}{\mathrm{Sin}\, E\ell + \dfrac{0.00143}{\tan E\ell + 0.0045}} \quad \cdots\cdots (20)$$

Table 6 (a) gives some basic conditions to calculate the effect of dry atmosphere, and Table 6 (b) shows the results of the calculations.

Table 6 (a) Calculated zenith path through neutral atomosphere for each station

Items	Kashima	MBS	OVRO
Height (m)	77 m	910 m	1205 m
Latitude	35.95°N	35.33°N	37.23°N
Gravity acc.	9.7759 m/s²	9.7731 m/s²	9.7739 m/s²
Pressure	1018.7 mb	909.8 mb	879.2 mb
Zenith excess path	2.321 m	2.073 m	2.003 m

Table 6 (b) Calculated excess delay along the line of sight to sources by using Chao's model

Observation	Kashima	MBS	OVRO
1. 4C39.25	7.93 nsec	17.05 nsec	15.29 nsec
2. 3C273b	14.62 nsec	12.91 nsec	12.38 nsec
3. 3C345	39.07 nsec	6.95 nsec	6.71 nsec
4. 3C273b	11.45 nsec	19.43 nsec	18.28 nsec

(2) Ionosphere: The zenith excess path I_Z is calculated by the next equation:

$$I_Z = 40.3 \frac{1}{c} \cdot \mathrm{TEC}/f_{RF}^2 \quad \cdots\cdots (21)$$

where TEC means the total electron contents in the unit-column along the line of sight, which is derived from the observed values of the critical frequency of F2-layer (f_0F_2) using "AFCRL mid-latitude TEC Model,"$^{(22)}$ and f_{RF} is the receiving frequency of X-band. The excess path I at the elevation Eℓ is given by the next equation:

$$I = \frac{I_Z}{\cos\left\{\sin^{-1}\left(\dfrac{R}{R + h_m} \cos E\ell\right)\right\}} \quad \cdots\cdots (22)$$

where R is the earth-radius and h_m is the mean height of F_2-layer (See Fig. 12). The derivation of Eq. (22) is shown in Appendix B.

Table 7 gives the calculated total electron content (TEC) and excess delay by using observed critical frequency of ionosphere (f_0F_2) along the line of sight.

Table 7 Total electron content (TEC) and excess delay calculated by using observed critical frequency of the ionosphere (f_0F2) along the line of sight

Observation	Kashima	MBS	OVRO
1. 4C39.25			
Elevation	77.1°	23.7°	25.6°
f_0F2	3.8 MHz	9.8 MHz	9.3 MHz
TEC	3.85×10^{16}	4.35×10^{17}	3.74×10^{17}
Excess delay	0.077 ns	0.866 ns	0.744 ns
2. 3C273b			
Elevation	31.8°	32.2°	32.6°
f_0F2	4.3 MHz	9.9 MHz	9.4 MHz
TEC	8.25×10^{16}	3.65×10^{17}	3.27×10^{17}
Excess delay	0.164 ns	0.727 ns	0.650 ns
3. 3C345			
Elevation	11.1°	84.0°	84.3°
f_0F2	5.2 MHz	9.9 MHz	9.4 MHz
TEC	1.70×10^{16}	2.16×10^{17}	1.95×10^{17}
Excess delay	0.339 ns	0.430 ns	0.388 ns
4. 3C273b			
Elevation	42.4°	20.6°	21.3°
f_0F2	6.6 MHz	9.9 MHz	9.4 MHz
TEC	1.35×10^{16}	4.81×10^{17}	4.25×10^{17}
Excess delay	0.269 ns	0.956 ns	0.847 ns

6. Observation Equation

6.1 Observable

The delay observable τ is given by the sum of the following terms:

$$\tau = \frac{1}{c}\left[\, P^T\, N^T\, S^T\, W^T\, \underline{B}_{fix} \right] \cdot \underline{s} + \Delta\tau_p + \sum_{k=1}^{K} \sum_{\ell=0}^{L} C_{k\ell}\, UT^{\ell}, \qquad \ldots\ldots\ldots\ldots\ldots (23)$$

where the first term called a geometrical delay τ_g is a scalar product of a baseline vector $\underline{B}$ (see Eq. (18)) at the inertial reference frame and a source-direction vector $\underline{s}$. The linearity of the observable τ with respect to $\underline{B}_{fix}$ is a big advantage of VLBI. In other method, namely the conventional geodesy or the satellite positioning, it is difficult to get a linear or simple expression between each of the observables and a baseline vector. Moreover, Eq. (23) does not need the information where the earth's origin exists. This allows us to use an arbitrary origin of the coordinates for VLBI data analysis. KAPRI in K-3 system adopted the position of Haystack as the reference point of VLBI coordinate system and other stations will be relatively determined from it.

The second term in Eq. (23) is the propagation effects mentioned in Sec. 5.3. This term is just additive to the geometrical delay τ_g.

The last term is called "clock polynomials". This term consists of the multi-segments indexed by k in Eq. (23) and of the multi-degrees indexed by ℓ in Eq. (23). The details of the clock polynomials are described in Sec. 6.3.

6.2 Partial Derivatives with Regard to Station-Position

The least square method to estimate a baseline vector requires the partial derivatives of delay with regard to the station-position. The baseline vector $\underline{B}_{fix}$ included in the first term of Eq. (23) is the difference between two position-vectors x_1 and x_2 for the two stations 1 and 2, respectively. In Eq. (23), we can include the nutation matrix N and the precession matrix P in the source-direction vector $\underline{s}$:

$$\underline{s}_t = NP\underline{s} \qquad \text{(24)}$$

In the following discussion, we consider the following simplified observation equation using the true source-direction of date $\underline{s}_t$. Thus,

$$\tau_g = -\frac{1}{c}[\, S^T W^T (\underline{X}_1 - \underline{X}_2)\,], \qquad \text{(25)}$$

where S and W are the diurnal rotation matrix and the wobbling matrix, given by:

$$S = \begin{pmatrix} \cos\theta & -\sin\theta & 0 \\ \sin\theta & \cos\theta & 0 \\ 0 & 0 & 1 \end{pmatrix} \qquad \text{(26)}$$

$$W = \begin{pmatrix} 1 & 0 & -w_x \\ 0 & 1 & w_y \\ w_x & -w_y & 1 \end{pmatrix}, \qquad \text{(27)}$$

where θ is GAST including UT1 as the form (UTC-UT1), and w_x and w_y are two components of the polar motion. Thus, the partial derivatives of delay with regard to $\underline{x}_1$ are:

$$\frac{\partial \tau_g}{\partial \underline{x}_1} = -\frac{1}{c} \begin{pmatrix} \cos\theta, \sin\theta, & w_x \cos\theta - w_y \sin\theta \\ -\sin\theta, \cos\theta, & -w_x \sin\theta - w_y \cos\theta \\ -w_x, \;\; w_y & 1 \end{pmatrix} \underline{s}_t \qquad \text{(28)}$$

Eq. (28) shows that the derivatives do not include the station-position explicitly and that they are absolutely the same for all pairs of baselines. Since w_x and w_y $\ll 1$, Eq. (28) is approximately equal to the next equation:

$$\frac{\partial \tau_g}{\partial \underline{x}_1} \doteqdot -\frac{1}{c} \begin{pmatrix} \cos\theta & \sin\theta & 0 \\ -\sin\theta & \cos\theta & 0 \\ 0 & 0 & 1 \end{pmatrix} \underline{s}_t \qquad \cdots\cdots\cdots (29)$$

6.3 Partial Derivatives with Regard to Clock Coefficients

The least square method for VLBI analysis always accompanies the estimation of clock parameters. The partial derivatives with regard to the k-th order clock parameters in ℓ-th clock-segment is simply given by the following equations (see Fig. 10):

$$\frac{\partial \tau_g (t)}{\partial C_{k\ell}} = \begin{cases} 0 \text{ (t is not in } \ell\text{-th segment.)} \\ UT^k \text{ (t is in } \ell\text{-th segment.)} \end{cases} , \qquad \cdots\cdots\cdots (30)$$

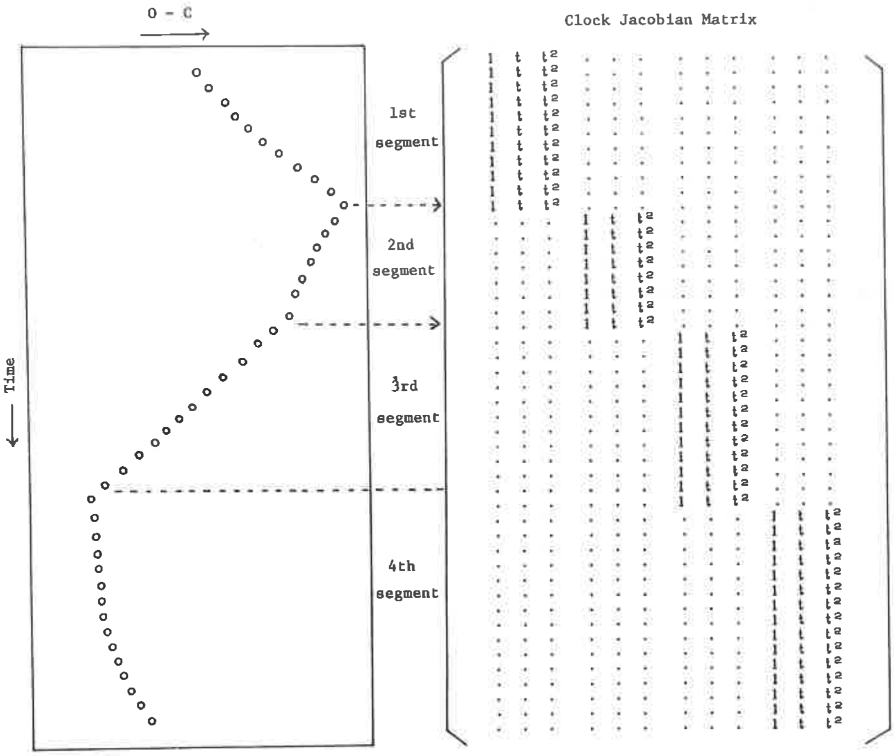

Fig. 10 Relation between residuals and the clock Jacobian matrix

where UT means Universal Time. Since the cross-correlation coefficients among the clock-parameters are often close to the value 1, it should be careful not to estimate too many clock parameters. In this analysis, one clock segment is estimated for three baselines, because the number of observations are limited.

6.4 Multi-baseline Jacobian Matrix

The observations of each baseline at one time are considered independent of each other. We can make the multi-baseline Jacobian matrix from one of single baselines. If A_S is a Jacobian matrix for a single baseline, the multi-baseline Jacobian matrix A for three baselines is given as follows:

$$A = \begin{pmatrix} A_S & 0 \\ 0 & A_S \\ A_S & -A_S \end{pmatrix} \qquad \cdots\cdots (31)$$

where 0 means a zero matrix. Since we consider the position of Mojave as a reference point for Kashima and Owens Valley, the first row is for Kashima-Mojave baseline, the second one is for Owens Valley-Mojave baseline and the last one is for Kashima-Owens Valley baseline, respectively. The left column is for the position and clock parameters of Kashima and the right one is for Owens Valley.

7. Least Square Method

7.1 Conventional Least Square Method

One begins with n observations which can be modeled by

$$\underline{Y} = \underline{\tilde{Y}} + \underline{y} + (\text{random S/N error } \underline{\sigma}), \qquad \cdots\cdots (32)$$

where $\underline{Y}$ is a "O"bserved-delay vector, $\underline{\tilde{Y}}$ is a "C"alculated-delay vector, y is a "O-C" vector and $\underline{\sigma}$ is a random error vector. The dimensions of all vectors are represented by n. One introduces a transformation f defined as follows:

$$\underline{Y} = f(\underline{X}) + \underline{\sigma} \qquad \cdots\cdots (33a)$$

and

$$\underline{\tilde{Y}} = f(\underline{\tilde{X}}), \qquad \cdots\cdots (33b)$$

where $\underline{X}$ and $\underline{\tilde{X}}$ are an estimation parameter vector and an a priori parameter vector, respectively. Their dimensions are all represented by m. When the a priori parameter is in the neighborhood of a true value, one can use the following approximation:

$$f(\underline{X}) = f(\underline{\widetilde{X}}) + \sum_{j=1}^{m} \frac{\partial f(X)}{\partial \widetilde{X}_j} (X_j - \widetilde{X}_j). \quad \cdots\cdots \quad (34)$$

The observation errors vector forms the error matrix Σ_y as follows:

$$\Sigma_y = \begin{pmatrix} \sigma_1{}^2 & & 0 \\ & \sigma_i{}^2 & \\ 0 & & \sigma_n{}^2 \end{pmatrix} \quad \cdots\cdots \quad (35)$$

Then, the weighting matrix W is given:

$$W = \begin{pmatrix} \frac{1}{\sigma_1{}^2} & & 0 \\ & \frac{1}{\sigma_i{}^2} & \\ 0 & & \frac{1}{\sigma_n{}^2} \end{pmatrix} = \Sigma_y^{-1} \quad \cdots\cdots \quad (36)$$

In this case, it is assumed that W is diagonal and that the errors are independent of each other.

If one uses the following vector-matrix notations,

$$\underline{x} = \underline{X} - \underline{\widetilde{X}} \quad \cdots\cdots \quad (37a)$$

$$\underline{y} = \underline{Y} - \underline{\widetilde{Y}} \quad \cdots\cdots \quad (37b)$$

$$y_i = Y_i - \widetilde{Y}_i = \sum_{i=1}^{m} A_{ij}\, x_j \quad \cdots\cdots \quad (38)$$

where

$$A_{ij} = \partial f_i(\underline{X}) / \partial \widetilde{X}_j\ , \quad (39)$$

the least square solution satisfies the next equation:

$$S(\hat{\underline{x}}) = \sum_{i=1}^{n} [y_i - \sum_{j=1}^{m} A_{ij}\, \hat{x}_j]^2 / \sigma_i{}^2 \ \rightarrow \text{Minimum} \quad \cdots\cdots \quad (40)$$

$$\frac{\partial S}{\partial \hat{x}_j} = -2 \sum_{i=1}^{n} [y_i - \sum_{j'=1}^{m} A_{ij'}\, x_{j'}] \frac{1}{\sigma_i{}^2} A_{ij} = 0 \quad \cdots\cdots \quad (41)$$

Then, Eq. (41) is rewrited into Eq. (42):

$$\sum_{i=1}^{n} (A_{ij}/\sigma_i{}^2)\, y_i - \sum_{i=1}^{n} \sum_{j'=1}^{m} A_{ij'} \frac{1}{\sigma_i{}^2} A_{ij}\, \hat{x}_{j'} = 0 \quad (42)$$

One makes the normal equation as follows:

$$A^T W \underline{y} = A^T W A \hat{\underline{x}} \quad \cdots\cdots \quad (43)$$

If the normal matrix B ($\equiv A^T WA$) is regular ($\det(B) \neq 0$), one gets the inverse matrix B^{-1} and the least square solutions $\underline{x}$:

$$\hat{\underline{x}} = B^{-1} A^T W\underline{y} \quad \ldots\ldots\ldots\ldots \quad (44)$$

SOLVE of Mark III software directly calculates the inverse matrix of B and gets the solutions as shown in Eq. (44). It is, however, often insufficient for this method to prevent the estimation from being correlative among the partial derivatives. SOLVE displays a correlation matrix and parameter-condition numbers mentioned in Sec. 7.3 to judge the quality of the estimation. An operator reselects the combination of parameters to minimize the condition numbers and the cross-correlation among the partial derivatives.

7.2 Q-R Method

As mentioned above, the partial derivatives are generally dependent on each other. By the use of the modified Gram Schmidt Method, we can resolve Jacobian matrix A into an orthogonal matrix Q and a triangle matrix R; this method is called "Q-R method".(23)

The following procedures make the new orthogonal vectors $\underline{z}^{(1)}, \underline{z}^{(2)}, \ldots \underline{z}^{(i)} \ldots \underline{z}^{(m)}$ from the arbitrary combination of linear independent vectors $\underline{p}^{(1)}, \underline{p}^{(2)}, \ldots \underline{p}^{(i)}, \ldots \underline{p}^{(m)}$:

$$\left.\begin{aligned} \underline{z}^{(1)} &= \underline{p}^{(1)} \\ \underline{z}^{(2)} &= \underline{p}^{(2)} - (\underline{p}^{(2)} \cdot \underline{z}^{(1)})\,\underline{z}^{(1)} \\ \underline{z}^{(3)} &= \underline{p}^{(3)} - (\underline{p}^{(3)} \cdot \underline{z}^{(1)})\,\underline{z}^{(1)} - (\underline{p}^{(3)} \cdot \underline{z}^{(2)})\,\underline{z}^{(2)} \end{aligned}\right\} \quad \ldots\ldots\ldots\ldots \quad (45)$$

In these procedures, the degree of the rank of $A = (\underline{p}^{(1)}, \ldots \underline{p}^{(m)})$ is easily determined by comparing the smallness of $|\underline{z}^{(i)}| / |\underline{p}^{(i)}|$ with the significant digits in the computer.

The normalization of $\underline{z}^{(1)}, \ldots \underline{z}^{(m)}$ produces the orthonormal vectors $\underline{q}^{(1)}, \ldots \underline{q}^{(m)}$ as follows:

$$\underline{q}^{(1)} = \underline{z}^{(1)} / |\underline{z}^{(1)}|, \ldots\ldots, \underline{q}^{(m)} = \underline{z}^{(m)} / |\underline{z}^{(m)}| \quad \ldots\ldots\ldots\ldots \quad (46)$$

Thus Q-R resolution of Jacobian A is given by the following equation:

$$A \equiv QR = (\underline{q}^{(1)} \ldots \underline{q}^{(m)}) \begin{pmatrix} r_{11} & \cdots & r_{1m} \\ & \ddots & \vdots \\ 0 & & r_{mm} \end{pmatrix}, \quad \ldots\ldots\ldots\ldots \quad (47)$$

where the components of matrix R are derived from the term of the scalar products $\underline{p}^{(i)} \cdot \underline{z}^{(j)}$ of Eq. (45).

As for the weighting, this resolution is applied to the weighted Jacobian matrix $W^{\frac{1}{2}} A$, namely:

$$W^{\frac{1}{2}} A \equiv QR \quad \ldots\ldots\ldots\ldots \quad (48)$$

substituting Eq. (48) into Eq. (43):

$$R^T Q^T W^{\frac{1}{2}} \underline{y} = R^T Q^T QR\underline{x} \tag{49}$$

$$= R^T R\underline{x} \tag{50}$$

$$R^T \underline{z} = R^T R\underline{x} \, , \tag{51}$$

where

$$\underline{z} = Q^T W^{\frac{1}{2}} \underline{y} . \tag{52}$$

After the determination of the rank of the weighted Jacobian matrix, one can make det (R) unequal to zero. One multiplies $(R^T)^{-1}$ to both sides of Eq. (51). Thus,

$$\underline{z} = R\hat{\underline{x}} . \tag{53}$$

Since R is a triangle matrix, R^{-1} is easily calculated by the inverse-substitution method. The least square solution $\hat{\underline{x}}$ is determined by:

$$\hat{\underline{x}} = R^{-1} \underline{z} \tag{54}$$

7.3 Covariance and Correlation Matrix

When the weighted Jacobian matrix is resolved into Q and R, it is easy to get the covariance matrix Σ_X, as follows:

$$\begin{aligned} \Sigma_X &= B^{-1} = (A^T WA)^{-1} \\ &= [R^T Q^T QR]^{-1} = R^{-1} (R^{-1})^T \end{aligned} \tag{55}$$

where R^{-1} is upper triangular and $(R^{-1})^T$ is lower triangular matrices. The diagonal elements of Σ_X are called as "formal errors" and the non-diagonal elements are used as "parameter condition numbers" in the following sections. The parameter condition numbers are simple indicators for the condition of least square estimation, used by Mark III group. If there are any big condition numbers, they considers that re-selection of parameters is necessary.

By Σ_X, the components ρ_{ij} of the correlation matrix C is given as follows:

$$\rho_{ij} = \frac{(\Sigma_X)_{ij}}{\sqrt{(\Sigma_X)_{ii} (\Sigma_X)_{jj}}} \tag{56}$$

8. Data Analysis

8.1 Analyzing Scenario

Fig. 11 (a) shows the differences between the observed delays in Table 4 and the high precision a priori delays described in Chapter 6. Since one baseline has four observations as shown in Table 4, it is at least possible to estimate X, Y, Z of Kashima and the clock offset of Kashima with regard to another station by the methods mentioned below. The scenario of the analysis consists of three steps:

(1) In Table 8, final residuals are calculated by the observed delays (O), ion-corrections (I), and calculated delays (C), namely (O+I–C). Fig. 11 (a) gives variations of the residuals along the time, and it shows that the clock of MBS with regard to other two stations has a rate-offset of about 4.9028×10^{-12} and that there is almost no difference in clock rate between Kashima and OVRO. Fig. 11 (b) shows the eliminated results of this rate-offset.

(2) Fig. 11 (b) suggests that Kashima's position probably has the differences of several-meters from their a priori values. Since this analysis, however, regards the a priori earth rotation parameters as unadjusted ones, some parts of the difference in Fig. 11 (b) might be caused by the errors of the earth rotation parameters. As the number of observations is small in this experiment, it is impossible to estimate the polar motions simultaneously. Here, the author considers the difference of Fig. 11 (b) caused only by the errors of Kashima's position.

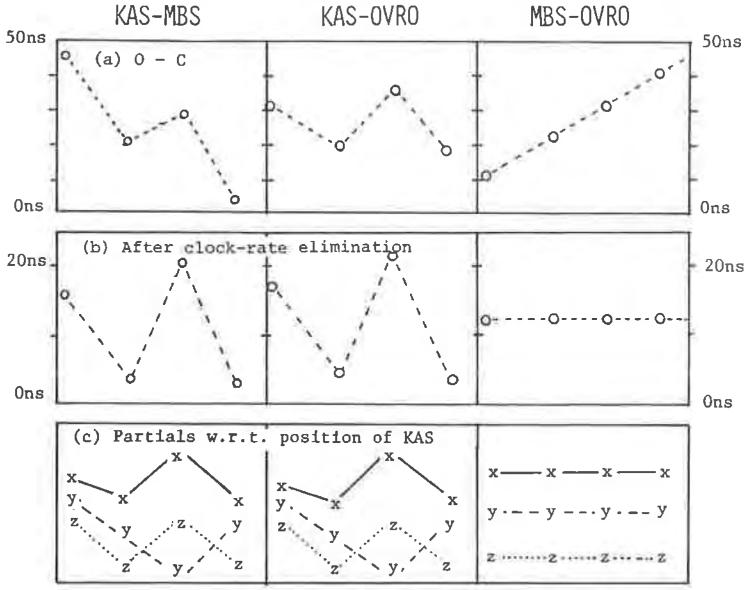

Fig. 11 (a) Residuals (Observed delay – Calculated delay)
Fig. 11 (b) Residuals after clock-drift elimination
Fig. 11 (c) Partial derivatives of delay with regard to (w.r.t.) position of Kashima

Table 8 Observed delays (O), ion correction (I), calculated delays (C), and "O + I − C"

(unit: nsec)

Obs #	Baseline	Observed delay (O)	Ion correction (I)	Calculated delay (C)	O + I − C
1	K − M	11,874,805.328	−0.789	11,888,754.21	−13,949.67
	K − O	11,237,436.866	−0.667	11,236,253.48	1,182.72
	M − O	−637,368.745	0.122	−652,510.43	15,141.81
2	K − M	−633,806.005	−0.563	−619,823.14	−13,983.43
	K − O	−686,765.918	−0.486	−687,936.58	1,170.18
	M − O	−52,960.046	0.077	−68,113.48	15,153.51
3	K − M	−17,343,635.191	−0.091	−17,329,659.69	−13,975.59
	K − O	−17,338,173.355	−0.049	−17,339,360.01	1,186.61
	M − O	5,461.533	0.042	−9,700.67	15,162.24
4	K − M	6,385,280.151	−0.687	6,399,280.87	−14,001.41
	K − O	6,181,594.724	−0.578	6,180,424.40	1,169.75
	M − O	−203,685.141	0.109	−218,856.22	15,171.19

Fig. 11 (c) shows the partial derivatives of τ_g with regard to the station position components X, Y, Z. $\frac{\partial \tau_g}{\partial x}$ and $\frac{\partial \tau_g}{\partial z}$ explain well the variation of Fig. 11. This means that a priori X and/or Z component of Kashima have/has errors of the order of several-meters. It is, however difficult to adjust X and Z components separately, because the partial's variation both of X and Z components are very similar, as shown in Fig. 11 (c).

Since the direction of baseline between Kashima and MBS/OVRO is almost along Y axis, X and/or Z components' errors are explained as the rotation errors of baseline.

(3) The errors of Kashima's position are calculated by the following four methods:

1. Simultaneous equation using four data of KAS-MBS
2. Simultaneous equation using four data of KAS-OVRO
3. Least square method for eight data of KAS-MBS and KAS-OVRO.
4. Closed least square methods using Eq. (46) for twelve data of KAS-MBS-OVRO.

8.2 Weighting

The weighting for the Jacobian matrix has two steps. In the first step, S/N random errors, calculated at the preprocessing stage, are directly used for weighting. At the second stage, the constant error σ_{add}, calculated by Newton-Raphson method, is added to S/N errors σ_{SN} in order to equalize the chi-square χ^2 of post-fit residuals to the degree of freedom as follows:

$$\chi^2 = \sum_{i=1}^{N} \frac{(y_i - \hat{y}_i)^2}{\sigma_{SN}^2 + \sigma_{add}^2} = n - m \quad \ldots\ldots\ldots\ldots\ldots\ldots\ldots\ldots\ldots\ldots\ldots (57)$$

This is a simple and convenient method to prevent the largeness of chi-square, used by Mark III group$^{(24)}$.

8.3 Solutions and Error Analysis

Two solutions in Table 9 (a) show the solutions of the simultaneous equations both for KAS-MBS and KAS-OVRO baselines. Since the degree of freedom is, of course, zero in the simultaneous equation, it is impossible to evaluate the errors of them. The difference between two independent solutions shows the systematic error between two methods; those are +/−28 cm, +/−23.5 cm, and +/−20 cm for three estimating parameters Δx, Δy and Δz, respectively.

Table 9 (b) also shows the four solutions by the least square method. First two solutions (indicated by "K-M" & "K-O" in Table 9 (b)) are resulted from the combination of two-baseline observations: K-M and K-O. Since eight observations are used to estimate five parameters (three positions: x_{KAS}, y_{KAS}, z_{KAS}, two clocks: $c_{KAS\text{-}MBS}$, and $c_{KAS\text{-}OVRO}$), the degree of freedom is three. In the first case, random errors caused by S/N are used to weight Jacobian matrix. In the second case, some additional errors are added to S/N errors as mentioned in Sec. 8.2. The chi-square χ^2 of the first case is 16.5 which is much larger than the degree of freedom: 3. This means that the weighting only by S/N errors must be underestimated to explain the residual errors. The root scaled-mean-square post-fit residuals (RSMS), defined by the following equation, is 2.35:

$$\mathrm{RSMS} = \sqrt{\chi^2 / (n - m)} \quad \ldots\ldots \quad (58a)$$

The scaled sigmas are defined by a following relation:

$$\sigma_{\mathrm{scaled}} = \mathrm{RSMS} \cdot \sigma_{\mathrm{formal}}, \quad \ldots\ldots \quad (58b)$$

where σ_{formal} is a formal error given by the covariance matrix. In this case σ_{scaled} covers the range from 9.4 cm to 25.1 cm for the positions and 0.89 ns for the time. These are comparable with the differences of the solutions of the simultaneous equations, mentioned above. The scaling method used in Eq. (58b) does not decrease RSMS to unity. The solutions, weighted only by S/N errors, are apt to overestimate the contribution of the coherence of radio sources to the residual errors. Some additional noises decrease their contributions. Thus the chi-square χ^2 becomes 2.23 which is around the degree of freedom 3, and RSMS becomes 0.862 which is near the unity, as shown in the second case of Table 9 (b). The scaled sigmas cover the range from 17.1 ns to 41.2 ns for positions and 1.45 ns for clocks.

Table 9 (a) Solutions by simultaneous equations

Parameters	KAS-OVRO	KAS-MBS
ΔX (cm)	181	237
ΔY (cm)	−31	16
ΔZ (cm)	581	541
$\Delta T_{K\text{-}O}$ (ns)	1175.1	–
$\Delta T_{K\text{-}M}$ (ns)	–	−13964.2
$B_{K\text{-}M}$ (cm)	809182360.0	809182363.0

Table 9 (b) Solutions by weighted least square methods.

Method	"K – M" & "K – O"		Closed three baseline	
Weighting	Only S/N	Add. noise	Only S/N	Add. noise
n (OBS #)	8	8	12	12
m (Parameters)	5	5	8	8
Chi-square	16.5	2.23	8.41	2.93
RSMS	2.35	0.862	1.45	0.856
X (cm)	195.0	207.0	143.0	110.0
formal	10.7	47.8	13.6	18.6
scaled	25.1	41.2	19.7	15.9
Y (cm)	–27.0	–24.0	9.0	–18.0
formal	4.0	19.8	5.3	7.5
scaled	9.4	17.1	7.7	6.4
Z (cm)	571.0	562.0	600.0	591.0
formal	9.0	36.0	11.0	14.5
scaled	21.2	31.0	16.0	12.4
$T_{K\text{-}O}$ (ns)	1175.5	1176.0	1175.0	1172.8
formal	0.38	1.68	0.48	0.65
scaled	0.89	1.45	0.70	0.56
$T_{K\text{-}M}$ (ns)	–13965.6	–13965.2	–13966.0	–13968.0
formal	0.38	1.68	0.48	0.65
scaled	0.89	1.45	0.70	0.56
$B_{K\text{-}M}$ (cm)	809,182,361.	809,182,361.	809,182,388.	809,182,387.
formal	6.4	32.4	22.3	19.2
scaled	15.0	27.9	32.3	16.4

Table 9 (b) also shows the case of solution for the closed least square method for three baselines. The degree of freedom is four, because twelve observations are used to estimate eight parameters. The chi-squares are 8.41 and 2.93 in the case of only S/N error and some additional errors, respectively. The scaled errors are about half of the two-baseline's ones. The estimated positions and clocks in Table 9 scatter between the range of +/–60 cm or +/–2.1 ns, respectively.

The error of baseline length σ_B is calculated by using the errors of X, Y and Z components, in consideration of the cross-correlations ρ_{ij} between parameters, as shown in Eq. (59):

$$\sigma_B{}^2 = \sum_{i=1}^{3} \sum_{j=1}^{3} \rho_{ij}\, \sigma_{x_i}\, \sigma_{x_j}\,, \qquad \text{(59)}$$

where ρ_{ij} is given by Eq. (56). The scaled sigmas of baseline length covers the range from 15 cm to 32 cm, as shown in Table 9 (b). The estimating lengths scatter between the range of +/–14 cm. The errors of earth-rotation parameters do not affect the length's error. The mutual independence of X and Z components produces only small effect on the length.

Thus, the baseline length is expected to be estimated with the accuracy of several decimeters by this analysis.

On the other hand, we can not make a hasty conclusion about the discrepancies of several-meters of position-vectors because of the mutual dependence of X and Z components. The following US/Japan experiment will decide the main cause of these discrepancies between the components of positions.

9. Discussion

The datum-shift of Eq. (60) should be applied to the transformation from Tokyo Datum to WGS-72(25), as mentioned in Appendix A:

$$U = -140.0 \text{ m}$$
$$V = +516.0 \text{ m} \qquad \cdots\cdots (60)$$
$$W = +673.0 \text{ m}.$$

The last case of Table 9 (b) requires further shift; the datum-shift correction becomes:

$$U = -138.1 \text{ m}$$
$$V = +515.8 \text{ m} \qquad \cdots\cdots (61)$$
$$W = +678.9 \text{ m}$$

Simosato Hydrographic Observatory reports the preliminary results of the shift correction from Tokyo Datum to the coordinate system LPM81.12 of SLR:(26)

$$U = -142.8 \text{ m}$$
$$V = +510.7 \text{ m} \qquad \cdots\cdots (62)$$
$$W = +681.0 \text{ m}$$

These two results are almost coincident to each other. To explain the several-meters difference between Eqs. (61) and (62), more observations of VLBI and SLR will be necessary.

The error-budgets in our results are discussed here. The errors of a priori ERPs contribute to improving the accuracy of the components of baseline. Meanwhile, the model error of propagation-effects affects both the components and the length of the baseline. The errors of ERPs from IPMS or BIH are expected to be around $0.01''$ for polar motions and 0.5 ms for UT1. Table 5 shows that they cause at most 0.168 ns (5.0 cm), 0.828 ns (24.8 cm) and 0.985 ns (29.6 cm) errors of delays with regard to the x and y components of polar motion and UT1, respectively.

The model errors of propagation effects cause the errors of calculated delay. The model errors of the zenith excess paths of dry atmosphere are around 7 ns and their model's accuracy is expected to be about +/−1.0 cm. The zenith excess paths of water vapor and ionosphere in that season are considered to be around 3.0 cm and 5.0 cm, respectively.

Table 10 summarizes the error-budget to be included in this analysis. Total r.m.s. error of this analysis is expected to be within +/−44.1 cm.

Table 10 Major error-budget for "decimeter-accuracy" of this experiment

ERPs	Maximum errors of ERP
Wobble-x	5.0 cm
Wobble-y	24.8 cm
UT1	29.6 cm

Propagation effects	Error at zenith path	Error at mean El (30°)
Water vapor	3.0 cm	5.9 cm
Dry atmosphere	1.0 cm	2.0 cm
Ionosphere	5.0 cm	8.9 cm

Total r.m.s. error by both ERPs and propagation	44.1 cm

10. Conclusion

The VLBI experiment conducted on Nov. 4, 1983, mentioned here, was the first trans-Pacific one, whose initial purpose was to confirm the coherence through the overall K-3 system. This paper shows that the results are also useful to calculate the baseline-length with an accuracy of several decimeters. This accuracy meant an epoch-making event as the direct geodetic measurement between Japan and the U.S.A. Moreover the coming VLBI experiments with one-day schedule will dramatically improve the precision and accuracy of the results. However, this experiment already included almost all subjects for the inter-continental experiment. This experiment presented us with a firm base of centimeter-baseline analysis for the coming experiments which will be more fruitful ones.

Other major results besides the one mentioned above are as follows:

(1) High-precision observed delays are determined by the techniques of K-3 cross-correlation (KROSS) and bandwidth synthesis (KOMB).

(2) Comprehensive and consistent a priori-physical models (KAPRI) enable us to calculate the accurate delays corresponding to the observed one.

(3) The new Q-R method is adopted for the baseline analysis. This will play an important role in the multi-baseline VLBI analysis.

(4) The chi-square test and the reweighting process produce reasonable results for the combinations of baselines.

Acknowledgement

This paper is cordially dedicated to all colleagues participating in the development of K-3 VLBI system at Kashima Branch of RRL, namely, J. Amagai, S. Hama, A. Kaneko, N. Kawaguchi, N. Kawano, H. Kiuchi, K. Koike, T. Kondo, S. Kozono, H. Kunimori, N. Kurihara, H. Kuroiwa, H. Murakami, Y. Sugimoto, K. Takahashi, Y. Takahashi, and T. Yoshino. I would like to acknowledge the strong support given by Mr. Y. Saburi, former

Associated Director General, and Drs. N. Kawajiri and K. Yoshimura in RRL Headquarters. I would also like to thank Drs. C. Ma, J. Ryan, B. Shupler, and T.A. Clark of GSFC/NASA, Dr. A.R. Whitney of Haystack Observatory and Dr. N. Vandenberg of Interferometrics Inc. for offering information about Mark III system and for close cooperation to perform the NASA/RRL joint VLBI experiment. I would also like to express my thanks to the staff members of International Latitude Observatory of Mizusawa and Geographic Survey Institute. I also acknowledge the valuable discussions with Dr. A. Tsuchiya of Tokyo Astronomical Observatory.

Appendix A.

Transformation from Tokyo Datum to VLBI coordinate

The position of Kashima-26 m antenna by Tokyo Datum (Besselian ellipsoid: $a = 6377397.155$ m, $f = 1/299.1528$) is:

$$\begin{array}{l} 35^\circ 57' 3.20'' \mathrm{N} \\ 140^\circ 39' 57.83'' \mathrm{E} \\ 45.18 \text{ m (height from ellipsoid)} \end{array} \quad \cdots\cdots \text{(A-1)}$$

or

$$\begin{array}{l} x = -3997745.50 \text{ m} \\ y = +3276072.85 \text{ m} \\ z = +3723438.44 \text{ m} \end{array} \quad \cdots\cdots \text{(A-2)}$$

The datum-shift from Tokyo Datum to WGS-72 is:

$$\begin{array}{l} U = -140.0 \text{ m} \\ V = +516.0 \text{ m} \\ W = +637.0 \text{ m.} \end{array} \quad \cdots\cdots \text{(A-3)}$$

Then, the position of Kashima-26 m antenna by WGS-72 is:

$$\begin{array}{l} x = -3997885.50 \text{ m} \\ y = +3276588.85 \text{ m} \\ z = +3724111.44 \text{ m.} \end{array} \quad \cdots\cdots \text{(A-4)}$$

The transformation from WGS-72 to VLBI coordinate is as follows:

$$\begin{array}{l} z = +4.0 \text{ m} \\ \text{Scale factor} = 3.263 \times 10^{-6} \\ \text{Rotation around Z-axis} = -0.54'' \end{array} \quad \cdots\cdots \text{(A-5)}$$

The position of Kashima-26 m by VLBI coordinate is:

$$\begin{array}{l} x = -3997895.36 \text{ m} \\ y = +3276579.46 \text{ m} \\ z = +3724116.67 \text{ m} \end{array} \quad \cdots\cdots \text{(A-6)}$$

Appendix B.

Calculation method of ionospheric excess path

The total electron content (TEC) is calculated from f_0F_2 (MHz) by "AFCRL mid-latitude TEC model":

$$\mathrm{TEC} = 1.24 \times 10^{13} (f_0 F2)^2 \left[261 + 26 \sin \frac{h-9}{12} \pi + K \sin \frac{D-60}{183} \pi \right] \quad \cdots\cdots \text{(B-1)}$$

where h is local time, D is a total day number and K takes the following values:

$$\left.\begin{array}{l} K = 73 \ (06h\text{–}19h \text{ Local time}) \\ K = 36 \ (05h \ \& \ 20h \text{ Local time}) \\ K = 0 \ \ (21h\text{–}04h \text{ Local time}) \end{array}\right\} \qquad \text{(B-2)}$$

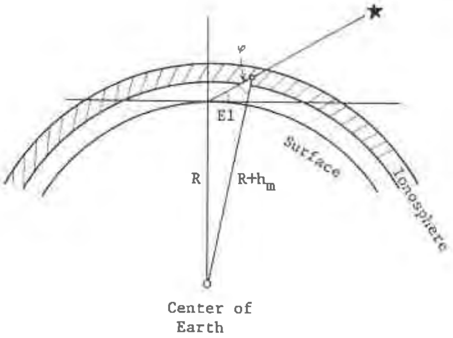

Fig. 12 Configuration of a radio-wave path in the ionosphere

Fig. 12 shows the configuration of a radio-wave path in the ionosphere. Elevation factor mentioned in Sec. 5.3 (2) is derived from:

$$\frac{R}{\sin \varphi} = \frac{R + h_m}{\sin \left(E\ell + 90^\circ\right)} \qquad \text{(B-3)}$$

where R is the earth's radius, h_m is a mean height of F_2 layer and φ is defined by Fig. 12. Thus, φ is:

$$\varphi = \sin^{-1}\left(\frac{R \cos E\ell}{R + h_m}\right) \qquad \text{(B-4)}$$

and the elevation factor is:

$$\frac{1}{\cos \varphi} = \frac{1}{\cos \left(\sin^{-1} \frac{R \cos E\ell}{R + h_m} \right)} \qquad \text{(B-5)}$$

References

(1) Rogers, A.E.E., Knight, C.A., Hinteregger, H.F., Whitney, A.R., Counselman III, C.C., Shapiro, I.I., Gourevich, S.A., and Clark, T.A.; "Geodesy by radio interferometry: detection of a 1.24-km base line vector with approx. 5-mm repeatability", J. Geophys. Res. 83, B1, 325, 1978.

(2) NASA Conference Publication 2115, "Radio interferometry techniques for geodesy", Proceeding of the conference held at MIT/Haystack Observatory, Westford, Massachusetts, June 19–21, 1979.

(3) Kawajiri, N., Ojima, T., Kawano, N., Takahashi, F., Yoshino, T., and Koike, K.; "The First VLBI Experiment in Japan", J. Radio Res. Lab., **26**, 119, pp. 13–64, 1979.

(4) Kawano, N., Takahashi, F., Yoshino, T., Koike, K., Kumagai, H., and Kawajiri, N.; "Development of real-time VLBI and measurements of scintillation", J. Radio Res. Labs., **29**, 127, pp. 53–102, 1982.

(5) Saburi, Y., Yoshimura, K., Kato, S., Imae, M., Morikawa, H., Sato, T., Takahashi, K., Kawajiri, N., Kawano, N., Takahashi, F., Kawaguchi, N., Koike, K., Yoshino, T., Sugimoto, Y., Kuroiwa, H., Kondo, T., Hama, S., Kunimori, H., Takahashi, Y., Murakami, H., Kurihara, N., Amagai, J., Kiuchi, H., Kaneko, A., and Kozono, S.; "The first US-Japan VLBI test observation by use of K-3 system developed at the Radio Research Laboratories" J. Radio Res. Labs. **31**, 132, pp. 31–37, March 1984.

(6) Takahashi, F., Yoshino, T., Murakami, H., Koike, K., Kunimori, H., and Kondo, T.; "K-3 VLBI software development for international experiment", Proceeding of IAG symposium No. 5: Geodetic application of radio interferometry, NOAA Technical Report, NOS 95, NGS 24, p. 177–183, 1982.

(7) Ma, C.; "Very long baseline interferometry applied to polar motion, relativity and geodesy", NASA Technical Memorandom 79582, 1978.

(8) Yoshino, T. and Koike, K.; "Part IV. K-3 VLBI Data Analysis Software, IV-2. The structure of data base system", Review Radio Res. Labs. **30**, Special Issue on "K-3 System development", (vernacular edition), Nov. 1984.

(9) Koike, K. and Yoshino, T.; "Part IV. K-3 VLBI Data Analysis Software, IV-4. Operating utilities for data base system", Review Radio Res. Labs. **30**, Special Issue on "K-3 "K-3 System development", (vernacular edition), Nov. 1984.

(10) Kunimori, H. and Hâma, H.; "Part III. K-3 VLBI Data Processing System, III-4. Cross-correlation and data acquisition software", Review Radio Res. Labs. **30**, Special Issue on "K-3 System development", (vernacular edition), Nov. 1984.

(11) Kondo, T. and Kunimori, H.; "Part III. K-3 VLBI Data Processing System III-5. Bandwidth synthesizing software (KOMB)", Review Radio Res. Labs. **30**, Special Issue on "K-3 System development", (vernacular edition), Nov. 1984.

(12) Kondo, T. and Yoshino, T.; "Part IV. K-3 VLBI Data Analysis Software, IV-8. Data transformation software (KONV)", Review Radio Res. Labs. **30**, Special Issue on "K-3 System development", (vernacular edition), Nov. 1984.

(13) Takahashi, Y. and Kondo, T.; "Part IV. K-3 VLBI Data Analysis Software, IV-3. Data base set-up software", Review Radio Res. Labs. **30**, Special Issue on "K-3 System development", (vernacular edition), Nov. 1984.

(14) Takahashi, Y. and Manabe, S.; "Part IV. K-3 VLBI Data Analysis Software, IV-5. A priori physical model software", Review Radio Res. Labs. **30**, Special Issue on "K-3 System development", (vernacular edition), Nov. 1984.

(15) Takahashi, F. and Yoshino, T.; "Part IV. K-3 VLBI Data Analysis Software, IV-6. Parameter estimation software", Review Radio Res. Labs. **30**, Special Issue on "K-3 System development", (vernacular edition), Nov. 1984.

(16) Whitney, A., "Precision geodesy and astronomy via very long baseline interferometry", M.I.T. Thesis for Ph.D., 1974.

(17) Amagai, J. and Hama, S.; "Part III. K-3 VLBI Data Processing System, III-3. Synchronization between two data recorders", Review Radio Res. Labs. **30**, Special Issue on "K-3 System development", (vernacular edition), Nov. 1984.

(18) Lieske, J.H.; "Expression for the precession quantities based upon the IAU (1976) system of astronomical constants", Astron. Astrophys. **58**, pp. 1–16, 1977.

(19) Wahr, J.M., "The tidal motions of a rotating, elliptical, elastic and oceanless earth", Univ. of Colorado, Thesis for Ph.D., 1979.

(20) Moran, J.M., Penfield, H.; "Test and evaluation of water vapor radiometers and determination of their capability to measure tropospheric propagation path length", report prepared for NASA Goddard Space Flight Center, 1976.

(21) Chao, C.C., A preliminary estimation of tropospheric influence on the range and range rate data during the closest approach of the MM71 Mars mission, Jet Propulsion Laboratory Tech. Memo. 391–129, 1970.

(22) Klobuchar, J.A. et al.; "Total electron contents studies of the ionosphere", AFGL-TR-73-0098, 1973.

(23) Nakagawa, T., and Koyanagi, Y.; "Experimental data analysis by least square method", (vernacular edition), Univ. of Tokyo Press, 1982.

(24) Ryan, J.W., Ma, C., and Vandenberg, N., R.; "The Mark III VLBI data analysis system", NASA X-945-80-25, 1980.

(25) Kaidzu, M., Private communication, 1983.

(26) Sasaki, M.; "Satellite Laser Ranging at the Simosato Hydrographic Observatory and its preliminary results", J. Geod. Soc. Japan, **30**, 1, pp. 29–40, 1984.